



Cite this: *New J. Chem.*, 2019, 43, 1313

Phthalazine-trione as a blue-green light-emitting moiety: crystal structures, photoluminescence and theoretical calculations†

Felipe Terra Martins,¹ Lauro June Queiroz Maia,² Gisane Gasparotto,² Ana Karoline Silva Medanha Valdo,² José Antônio Nascimento Neto,² Leandro Ribeiro,² Yuri de Freitas Rego,³ Cleiton Moreira da Silva³ and Ângelo de Fátima³

Phthalazine (2,3-diazanaphthalene) and phthalhydrazide (2,3-dihydro-1,4-phthalazinedione) compounds are heterocycles with several biological properties. Most recently, analogous phthalazine-triones also emerged as drug candidates. Herein, we introduced a phthalazine-trione moiety as a promising fluorophore in the blue and green spectral regions. This desired optical property was rationalized based on their crystal structure and time-dependent density functional theory (TD-DFT) calculations. Under ultraviolet (UV) excitation (ca. 360 nm), two light emission maxima at ca. 460 nm and 480 nm were observed for ten phthalazine-triones, regardless of the substitution pattern. This conservation in the light-emitting property was rationalized by our time-dependent DFT calculations for the three phthalazine-triones whose crystal geometries were also determined in this study (4-chlorophenyl, 3-methoxyphenyl and 4-nitrophenyl derivatives) and for those available in literature (4-fluorophenyl and 4-bromophenyl derivatives). Electronic transitions with the largest oscillator strengths were near 360 nm and were in excellent agreement with the experimental excitation energy (UV-visible and photoluminescence spectra). Lifetime values of selected samples could also be determined, which were between 1.59 ns and 3.21 ns. In all compounds, the Frontier molecular orbitals involved in these excitations were distributed over the phthalazine-trione moiety and were not localized on the changeable substituent.

Received 14th June 2018,
Accepted 3rd December 2018

DOI: 10.1039/c8nj02976h

rsc.li/njc

Introduction

Phthalazine (2,3-diazanaphthalene) and phthalhydrazide (2,3-dihydro-1,4-phthalazinedione) derivatives are heterocycles containing hydrazine moieties. Compounds containing these structures have shown significant biological and pharmacological activities such as antifungal,¹ VEGFR-2 inhibitor,² vasorelaxant,³ cardiotoxic,⁴ and antiproliferative.⁵ Additionally, these heterocycles also have interesting luminescent properties (Fig. 1).⁶ Phthalazine-BF₂ complex (A) displayed blue phosphorescence when subjected to UV radiation.⁷ Cyclometalated benzo[g]phthalazine iridium(III) complex (B) was reported to

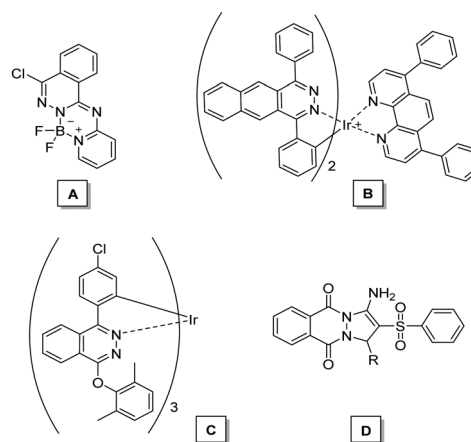


Fig. 1 Phthalazine derivatives presenting luminescent properties.

^a Instituto de Química, Universidade Federal de Goiás, Campus Samambaia, CP 131, Goiânia, GO, 74001-970, Brazil. E-mail: felipe@ufg.br

^b Instituto de Física, Universidade Federal de Goiás, Campus Samambaia, CP 131, Goiânia, GO, 74001-970, Brazil

^c Grupo de Estudos em Química Orgânica e Biológica (GEQOB), Departamento de Química, Instituto de Ciências Exatas, Universidade Federal de Minas Gerais, Av. Pres. Antônio Carlos, 6627, Belo Horizonte, MG, 31270-901, Brazil

† CCDC 1836431–1836433. For crystallographic data in CIF or other electronic format see DOI: 10.1039/c8nj02976h

exhibit near-infrared-emitting phosphorescence.⁸ Polymer light-emitting devices doped with the iridium(III) complex (C) showed high photoluminescence quantum efficiency of 96%.⁹ Luminescence was also noted in highly functionalized

phthalazine-dione derivatives (**D**), which exhibited fluorescence at 486–492 nm.¹⁰ These luminescence properties could be harnessed into new and more efficient technologies such as organic light-emitting diodes (OLEDs), phosphorescent organic light-emitting diodes (PhOLEDs), laser dyes and luminescent materials.

Recently, 2*H*-indazolo[2,1-*b*]phthalazine-trione derivatives were synthesized by microwave-assisted one-pot three-component condensation reaction using *p*-sulfonic acid calix[4]arene as catalyst and green solvents.⁵ Even though the exploration of their medicinal properties has begun, no other technological application has been reported thus far. Herein, we present a detailed study of the crystalline structure and luminescence properties of phthalazine-triones, which could be understood based on density functional theory (DFT) calculations. Phthalazine-trione was found to be a new robust blue-green light-emitting fluorophore, regardless of the substitution pattern.

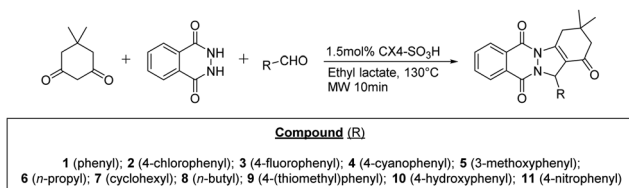
Experimental

Synthesis

Phthalazine-triones **1–11** (Scheme 1) were synthesized according to the literature.⁵ Briefly, 1.0 mmol of phthalhydrazide, 1.2 mmol of dimedone, 1.5 mmol of aldehyde and 1.5 mol% of *p*-sulfonic acid calix[4]arene were mixed in 1.0 mL of ethyl lactate. The mixture was heated under microwave radiation at 130 °C for 10 minutes. After cooling to room temperature, water was added. Then, the solution was cooled to –20 °C for precipitation. The solid was filtrated and purified by silica gel column chromatography.

Single crystal X-ray diffraction

Suitably sized single crystals of **2**, **5** and **11** were obtained and exposed to an X-ray beam using a Bruker-AXS Kappa Duo diffractometer with an APEX II charge-coupled device (CCD) detector (Cu K α radiation, 296 K). Bruker programs, SAINT and SADABS,¹¹ were used for cell refinement and data indexing, integration and reduction. Multi-scan absorption correction was performed for our Cu K α dataset.¹² Structure solution and refinements were performed using SHELXL-2014¹³ within WinGX.¹⁴ Structure analysis and artwork preparation were performed with mercury¹⁵ and ORTEP-3.¹⁶ Non-hydrogen and hydrogen atoms were refined anisotropically and isotropically, respectively. All CH hydrogens were added to their corresponding carbons following a riding model with fixed bond angles and lengths (0.93 Å, 0.96 Å, 0.97 Å and 0.98 Å in aromatic, methyl, methylene and methine groups, respectively).



Scheme 1 General synthesis of phthalazine-triones.

Hydrogens had their isotropic atomic displacement parameters set to $1.2U_{\text{iso}}(\text{C})$, except in the case of methyl groups where this value was $1.5U_{\text{iso}}(\text{C})$. The complete X-ray diffraction dataset for all structures is available under the CCDC number codes shown in Table 1, wherein a summary of X-ray diffraction data is also presented.

Photoluminescence (PL) and lifetime measurements

PL excitation and emission spectra were recorded using a double monochromator and a Hamamatsu photomultiplier tube as the detector (Fluorolog FL3-221 from Horiba Jobin-Yvon), under excitations from a Xe arc lamp delivering 450 W. The bandpass was fixed at 0.5 nm and readings were recorded every 1.0 nm. The PL measurements were performed in both crystals and the chloroform solution. PL decay curves were collected at 475 nm with a bandpass of 6 nm for selected compounds in a chloroform solution, under an excitation at 390 nm from a NanoLED source operating at 1 MHz with 1.2 ns pulse duration.

Theoretical calculations

In order to rationalize the conformational features and the strong photoluminescence observed for phthalazine-triones, we performed DFT calculations^{17,18} with full optimization for the crystal geometries reported here and those available in the literature (F and Br analogs)^{5,19} at the B3LYP/6-31G(d,p) level of theory.^{20,21} Next, Frontier molecular orbitals (FMOs) and time-dependent DFT (TD-DFT) calculations were carried out at the same level of theory by inputting the fully optimized geometries. Frequency calculations confirmed the nature of the located stationary point. For all structures, positive definite Hessian matrices were found. All calculations were accessed with the Gaussian 09 program package.²²

Results and discussion

Suitably shaped single crystals of **2**, **5** and **11** were successfully obtained from exhaustive crystallization assays. Even though C15 is a chirality center, all compounds crystallized in centrosymmetric space groups ($P2_1/n$ for **2**, $P2_1/c$ for **5** and **11**), *i.e.*, both enantiomers were present in the racemic crystals. In compliance with the structure elucidation studies already reported in the literature for the analogs, the *S* enantiomer was chosen to be the crystallographic asymmetric unit as well as atom labeling scheme followed that of the F analog.⁵ Before this study, the crystal structure was determined for the other two phthalazine-triones that differed from **2** only by the halogen atom in the *para* position of phenyl ring attached at C15. One of these two literature analogs, namely, that bearing Br {13-(4-bromophenyl)-3,3-dimethyl-2,3,4,13-tetrahydro-1*H*-indazolo[1,2-*b*]phthalazine-1,6,11-trione;¹⁹ herein after numbered as **12** even though it was not synthesized by us} is isostructural to our chlorinated compound **2**. Both have the same molecular conformation, crystal packing, similar unit cell parameters and an equal space group. In contrast, the literature antecedent owning F in lieu of Cl/Br {13-(4-fluorophenyl)-3,3-dimethyl-2,3,4,13-tetrahydro-1*H*-indazolo[1,2-*b*]phthalazine-1,6,11-trione}⁵ differs by its intermolecular arrangement and therefore

Table 1 Summary of crystal data and refinement statistics for phthalazine-triones elucidated in this study

	2	5	11
Structural formula	C ₂₃ H ₁₉ ClN ₂ O ₃	C ₂₄ H ₂₂ N ₂ O ₄	C ₂₃ H ₁₉ N ₃ O ₅
Space group	P2 ₁ /n	P2 ₁ /c	P2 ₁ /c
Z/Z'	4/1	4/1	4/1
a (Å)	6.2427(2)	16.4477(4)	5.7534(7)
b (Å)	13.2218(4)	7.3740(2)	18.2637(17)
c (Å)	24.3513(8)	16.5927(4)	18.7499(19)
β (°)	93.176(2)	97.642(2)	98.750(8)
V (Å) ³	2006.86(11)	1994.58(9)	1947.3(4)
Calculated density (mg m ⁻³)	1.347	1.340	1.424
θ range for data collection (°)	3.636–66.545	2.710–66.573	3.397–66.776
Data collected	9240	9844	8457
Unique reflections	3421	3432	3242
Unique reflections with I > 2σ(I)	2232	2593	1920
Symmetry factor (R _{int})	0.0492	0.0329	0.0458
Parameters refined	262	271	281
Goodness-of-fit on F ²	1.029	1.030	1.071
Final R ₁ factor for I > 2σ(I)	0.0483	0.0441	0.0644
wR ₂ factor for all data	0.1352	0.1225	0.2124
Largest Δρ peaks (e Å ⁻³)	0.238/–0.252	0.156/–0.235	0.275/–0.288
CCDC	1836431	1836433	1836432

unit cell constants, even though it crystallizes in the same space group as its related halogenated analogs. Only this halogen replacement was enough to profoundly change the pattern of weak intermolecular contacts, which was also related to a slight conformational change in the halogen-substituted phenyl ring (see below).

Only one molecule was found in the asymmetric unit of the two known phthalazine-triones and the three phthalazine-triones elucidated here. The non-hydrogen atom and ring labeling scheme is shown in Fig. 2.

In the F analog, the average plane of the halogen substituted phenyl ring E transversely crossed the five membered heterocycle C. The imaginary plane formed with C16, C15 and the centroid of the N2–C9 (C_g_{N2–C9}) bond formed a dihedral angle of 4.87° with the F-substituted phenyl ring (Table 2). The N1–C15–C16–C17 torsion also helped to describe this conformational feature [61.57(15)°]. This phenyl ring, which was already in the Cl/Br derivatives and also the *meta*-methoxy derivate 5, was slightly bent towards the nitrogen due to the rotation on the C15–C16 bond axis. The aforementioned dihedral angle measured 17.10°/17.34° and 21.60° in such compounds, respectively, while the N1–C15–C16–C17 torsion was 43.1(3)°/43.1(4)° and 37.7(2)°.

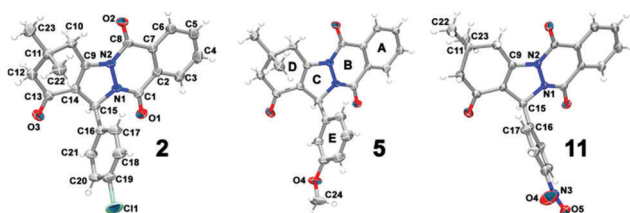


Fig. 2 Asymmetric unit of the phthalazine-triones reported in this study. Non-hydrogen atoms are drawn with their 30% probability ellipsoid, while hydrogen atoms are arbitrary radius spheres. The labelling scheme of the non-hydrogen atoms and rings common to all compounds followed those shown once. For clarity, the labelling of key atoms used in the conformational descriptions was repeated in **11**.

Table 2 Selected conformational descriptors (in °) for the phenyl ring E twist in theoretical and crystal geometries (C_g_{N2–C9} denotes the centroid calculated for these atoms)

Compd	Angle between the planes					
	C16–C15–C _g _{N2–C9} and C16 to C21			N1–C15–C16–C17 torsion		
	Crystal	DFT C11-endo	DFT C11-exo	Crystal	DFT C11-endo	DFT C11-exo
2	17.10	28.18	17.84	43.1(3)	30.70	74.08
3	4.87	25.10	18.42	61.6(2)	33.83	74.70
5	21.60	17.25	16.11	37.7(2)	41.43	42.55
11	30.89	30.68	30.73	85.9(4)	28.08	28.06
12	17.34	28.45	17.99	43.1(4)	30.42	74.21

Interestingly, in the nitro compound **11**, the phenyl ring was also slightly twisted relative to the imaginary plane transversal to the five-membered ring (the corresponding angle between these planes was 30.89°), but towards the opposite side of the heterocyclic nitrogens [N1–C15–C16–C17 = 85.9(4)°]. This conformational feature was seemingly associated with the cyclohexenone puckering. In the solid state of all phthalazine-triones, cyclohexenone adopted the half-chair conformation, with C11 lying away from the other five coplanar atoms (C10–C9–C14–C13–C12 r.m.s.d. = 0.0489 Å, 0.0217/0.202 Å, 0.0495 Å and 0.0512 Å in F, Cl/Br, *meta*-methoxy and *para*-nitro derivatives, respectively). In all these structurally elucidated phthalazine-triones, C11 was puckered on the same side of the phenyl ring E relative to the phthalazine-trione mean plane, describing a C11-endo conformation. On the contrary, C11 in **11** deviated from this least-square plane, but pointed towards the opposite side of the substituted phenyl ring in a so-called C11-exo pucker (Fig. 2 and 3). In this last structure, C22 and C23 methyl carbons occupied equatorial and axial positions, respectively. In F/Cl/Br/MeO analogs, C22 and C23 were instead in axial and equatorial positions.

In order to probe the conformational preference for the phthalazine-triones as a function of the phenyl ring E substitution pattern, we full-optimized the crystal geometries reported

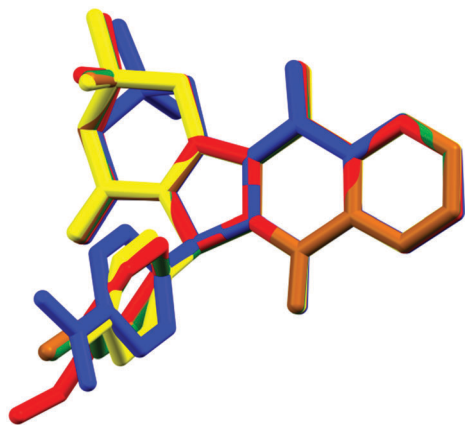


Fig. 3 Molecular superimposition for **2** (green), **5** (red) and **11** (blue), all determined here, and for the literature analogs, **3** (yellow) and **12** (brown).^{5,19}

here and those available in the literature (F and Br analogs)^{5,19} and their corresponding conformers with the opposed cyclohexenone puckering upon flipping C11 through the average chair plane of ring D. Two minimal energy conformers bearing C11 on opposite sides of ring D were found for all five compounds, which had practically equal energies differing by less than 0.13 kcal mol⁻¹. For halogenated derivatives, the conformation around C15–C16 followed the conformation found in the solid state. Accounting for the phthalazine-trione plane, if C11 was on the same side of ring E, the last was slightly bent towards the heterocyclic nitrogens (see Table 2 for values of these conformational descriptors). This additionally reveals that the alignment of the ring E mean plane with the transversal plane of ring C was a consequence of the intermolecular contacts assembled by the F-substituted phenyl ring (see below). The conformational descriptors for the phenyl ring twist differed between the crystal and theoretical C11-*endo* geometries (Table 2). The theoretical conformational parameters of the F analog resembled those of the Cl/Br parents (Table 2). If C11 was on the opposite side of ring E, the last was twisted in an opposed direction to the heterocyclic nitrogens (Table 2). Interestingly, this conformational relationship between the cyclohexenone puckering and the phenyl twist found theoretically in the gas phase of the halogenated derivatives, which occurred also in the solid state, was not experienced in **11** and **5** in the gas phase. For these two compounds, the phenyl ring E was twisted towards the heterocyclic nitrogens in both minimal energy points, regardless of the C11 puckering mode. This shows that the rotation on the C15–C16 is due to intermolecular interactions adopted by the nitrophenyl ring as described in the sequence. In Table 2, the angle between the planes crossing through C16–C15–Cg_{N2-C9} and C16 was similar in both C11-*endo* and C11-*exo* theoretical conformers, as well as their values of the N1–C15–C16–C17 torsion do not differ significantly.

Another striking conformational feature is the high coplanarity of the four fused rings in the halogen-based compounds (except for C11). The r.m.s.d. values for the least-square plane fitted through the sixteen atoms C1 to C10, C12 to C15, N1 and

N2 were lower in the F/Cl/Br derivatives [0.0710/0.0574/0.0495 Å, largest deviations of 0.1504(12)/0.103(3)/0.094(4) Å for C10 in F analog and C13 in both Cl/Br analogs] than in **5** [0.190 Å, largest deviation of 0.438(2) Å for C12] and **11** [0.235 Å, largest deviation of 0.376(5) Å for C4]. These last two phthalazine-triones underwent a ruffling in their molecular plane formed with the four fused rings. Rings A and B formed a plane slightly inclined out compared with that formed with rings C and D (the angle between the planes crossing through rings A/B and C/D (except C11) was 2.90(4)/2.90(3)/2.37(6)°, 12.12(3)° and 16.05(7)° in the F/Cl/Br analogs and in *meta*-methoxy and *para*-nitro analogs, respectively).

The crystal packing of the Cl/Br derivatives had chains composed of 2₁-screw axis symmetry-related molecules arrayed in a zigzag fashion along the *b* axis (Fig. 4). Within these chains, the main intermolecular interactions are CH...O non-classical hydrogen bond assembling R₂²(10) motifs. Both carbonyl groups from the phthalazine framework and their vicinal aromatic CH

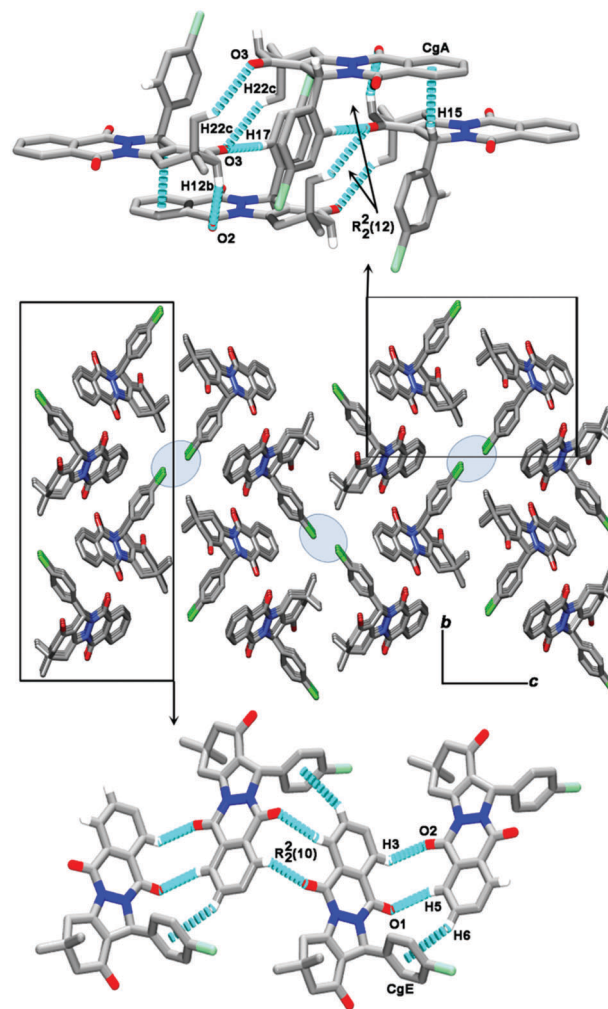


Fig. 4 Overall crystal packing of **2** and details of the main intermolecular interactions. Circled regions denote the halogen...halogen interactions. Cg denotes the centroid calculated through the non-hydrogen endocyclic ring atoms. The succeeding capital letter refers to the ring as labeled in Fig. 2. Also, for clarity, only CH hydrogens involved in the displayed contacts will be shown.

groups were engaged in the formation of the supramolecular ring motif (Fig. 4). T-shaped $\text{CH}\cdots\pi$ contacts between one CH moiety from phthalazine and the π -system from the phenyl ring E helped to stabilize the primarily hydrogen bonded $\text{CH}\cdots\text{O}$ chains. These chains were further face-to-tail stacked along the a axis on top of each other by means of $R_2^2(12)$ motifs and $\text{CH}\cdots\pi$ interactions. Again, these ring motifs were composed of two $\text{CH}\cdots\text{O}$ non-classical hydrogen bonds having one methylene group and one CH moiety from the substituted phenyl ring as donors to the carbonyl oxygen from phthalazine and cyclohexenone. This additional $\text{CH}\cdots\pi$ interaction engaged the methine CH and the benzene moiety from phthalazine. Another $R_2^2(12)$ graph set enclosed by the methyl and cyclohexenone carbonyl groups was found along the a axis between molecules that were not directly stacked on top of each other (Fig. 4). The geometry of all discussed intermolecular contacts are grouped in Table 3 for the phthalazine-triones determined here and the F analog.⁵

$R_2^2(12)$ motifs were also found in the F derivative (Fig. 5). However, these were formed with one $\text{CH}\cdots\text{F}$ non-classical hydrogen bond and another $\text{CH}\cdots\text{O}$ non-classical hydrogen bond. These motifs assembled chains running along the [101] direction. These chains are now face-to-face stacked along the b axis on top of each other through $\pi\cdots\pi$ interactions (Fig. 5). The carbonyl group from cyclohexenone accepted hydrogen bonds from methine, in which two centrosymmetric interactions gave rise to another $R_2^2(10)$ motif and one CH moiety belonging

Table 3 Geometry of selected main intermolecular contacts found in phthalazine-triones determined here and in the literature analog 3^5

Compd	D-H...A	D-H (Å)	H...A (Å)	D...A (Å)	D-H...A (°)
2	C3-H3...O2	0.93	2.47	3.077(3)	123
	C5-H5...O1	0.93	2.66	3.569(3)	166
	C12-H12b...O2	0.97	2.59	3.361(3)	137
	C17-H17...O3	0.93	2.41	3.333(3)	174
	C22-H22c...O3	0.96	2.72	3.558(3)	146
	C6-H6...CgE	0.93	2.95	3.774(3)	148
	C15-H15...CgA	0.98	2.66	3.506(2)	144
	Cl1...Cl1	—	—	3.8567(15)	—
3	C5-H5...O3	0.93	2.39	3.085(2)	130
	C15-H15...O3	0.98	2.58	3.533(2)	160
	C17-H17...F1	0.93	2.57	3.390(2)	145
	C18-H18...O2	0.93	2.53	3.424(2)	157
	CgA...CgB	—	—	3.581(2)	—
5	C6-H6...O1	0.93	2.57	3.234(2)	129
	C12-H12b...O1	0.97	2.49	3.416(2)	160
	C15-H15...O2	0.98	2.51	3.477(2)	168
	C23-H23c...O3	0.96	2.70	3.578(3)	149
	C12-H12a...CgE	0.97	2.92	3.762(2)	146
	C23-H23a...CgA	0.96	3.14	3.985(2)	148
	CgA...CgB	—	—	3.524(2)	—
11	C5-H5...O3	0.93	2.38	3.294(6)	167
	C10-H10a...O5	0.97	2.57	3.452(5)	151
	C6-H6...CgE	0.93	3.13	3.915(4)	144
	C18-H18...CgA	0.93	3.09	3.589(4)	116
	O1...C1	—	—	3.119(5)/3.141(5)	—
	O2...N3	—	—	2.873(5)	—
	O4...C8	—	—	3.098(6)	—

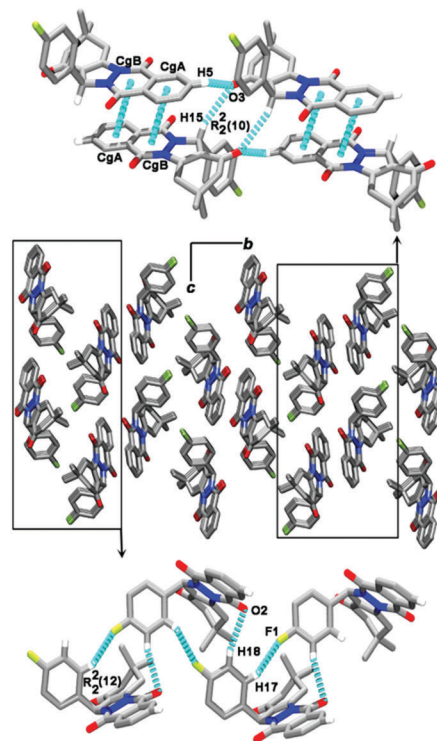


Fig. 5 Overall crystal packing of **3** and details of its main intermolecular interactions.⁵

to phthalazine, thus completing the three-dimensional crystal packing through the assembly of chains along the c axis. Therefore, just the Cl/Br substitution for F altered much of the intermolecular ordering in the phthalazine-triones despite the reduced impact from conformational changes. Due to its highest electronegativity, fluorine was involved in non-classical hydrogen bonding, while Cl/Br were interacting with themselves in halogen...halogen contacts (Fig. 4).

The $\text{CH}\cdots\text{O}$ hydrogen bonded $R_2^2(10)$ motifs described before in Cl/Br derivatives were also found in **5**, but the translation symmetry molecules were chained along the b axis in the last (Fig. 6).

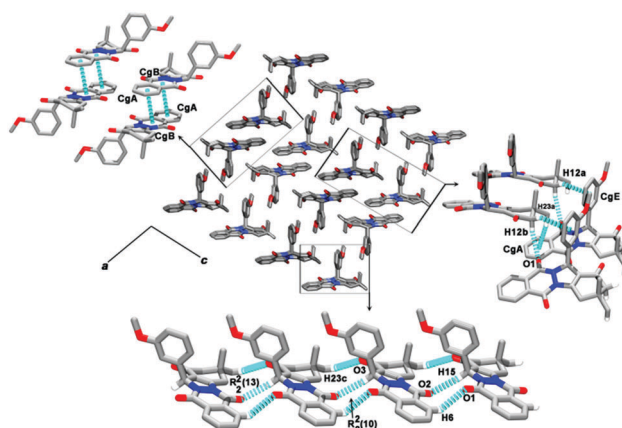


Fig. 6 Overall crystal packing of **5** and details of its main intermolecular interactions.

In addition, the methine group substituted one aromatic CH as the donor in **5**. Another $\text{CH}\cdots\text{O}$ non-classical hydrogen bond involving one methyl and carbonyl group from cyclohexenone contributed to keep **5** molecules in contact with these chains,

giving rise to a $R_2^2(13)$ moiety (Fig. 6). The cross-linking among neighboring chains was from $\pi\cdots\pi$ contacts on a side of the phthalazine average plane and from $\text{CH}\cdots\text{O}$ and $\text{CH}\cdots\pi$ on another side (Fig. 6).

While there was a parallel disposition of molecules into chains for all conformationally similar phthalazine-triones, **11** molecules had their phthalazine and nitro substituted phenyl planes oriented almost perpendicular due to dipolar interactions between one phthalazine carbonyl group and one nitro group (Fig. 7). Additionally, the two $\text{CH}\cdots\text{O}$ interactions between one phthalazine CH group and the cyclohexenone oxygen as well as between one CH_2 group and the nitro group acted for assembling $R_2^2(19)$ motifs between these $\text{O}\cdots\text{N}$ interacted molecules. All these contacts kept the molecules onto molecular layers, extending infinitely along the (010) plane. T-shaped $\text{CH}\cdots\pi$ contacts were also identified on these molecular layers (Fig. 7). Another dipolar interaction between the phthalazine carbonyl groups was responsible for the face-to-tail stacking of the molecules along the *a* axis (Fig. 7).

In Fig. 8, the PL emission spectra of the phthalazine-triones are presented under an excitation wavelength around 360 nm. A broad band emission between 420 nm and 550 nm (blue and green emissions), with two maxima at *ca.* 460 nm and 480 nm and one shoulder at *ca.* 510 nm, was observed for some compounds structurally studied here (F, Cl and MeO analogs) and others previously synthesized.⁵ Slight shifts (up to 5 nm) in the excitation wavelengths as well as the maxima and shoulder emission wavelengths were found as a result of the substituent at C15. However, the emission pattern was conserved in all light emitting phthalazine-triones, revealing

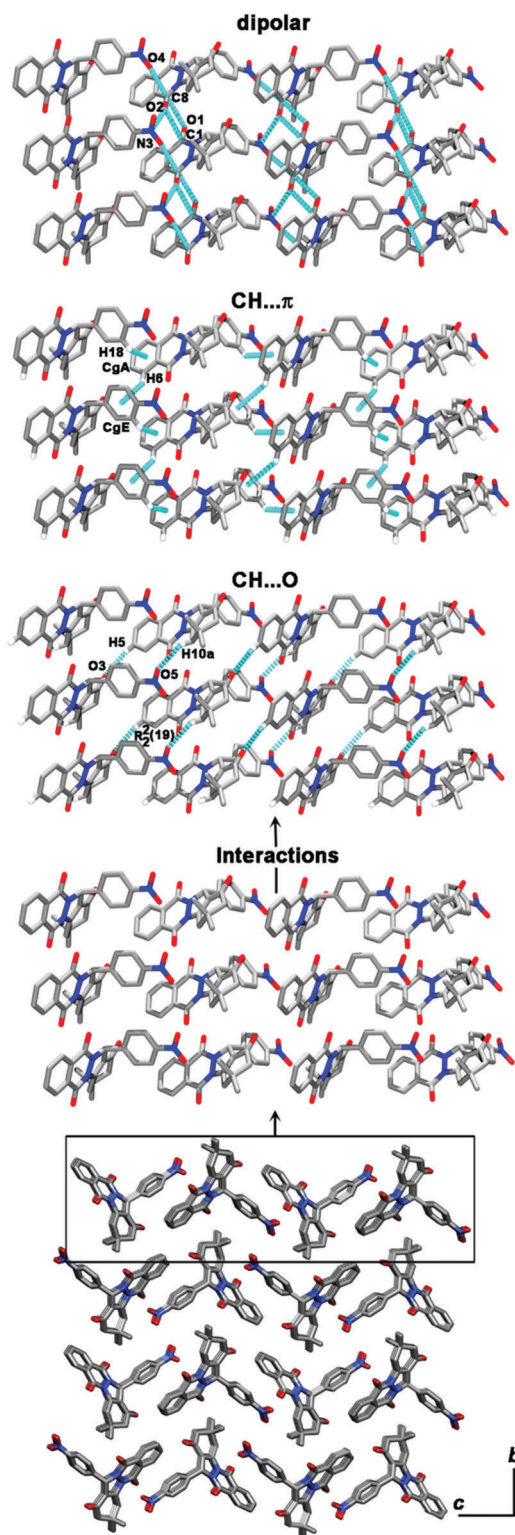


Fig. 7 Overall crystal packing of **11**, the molecular layer formed onto the (010) plane and details of the main intermolecular interactions found there.

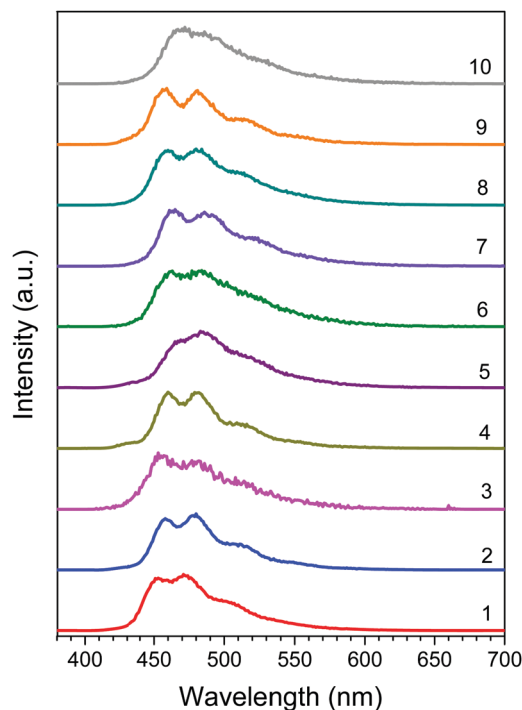


Fig. 8 PL emission spectra for phthalazine-triones under excitation of 360 nm.

that such a solid-state property came from their common molecular moiety.

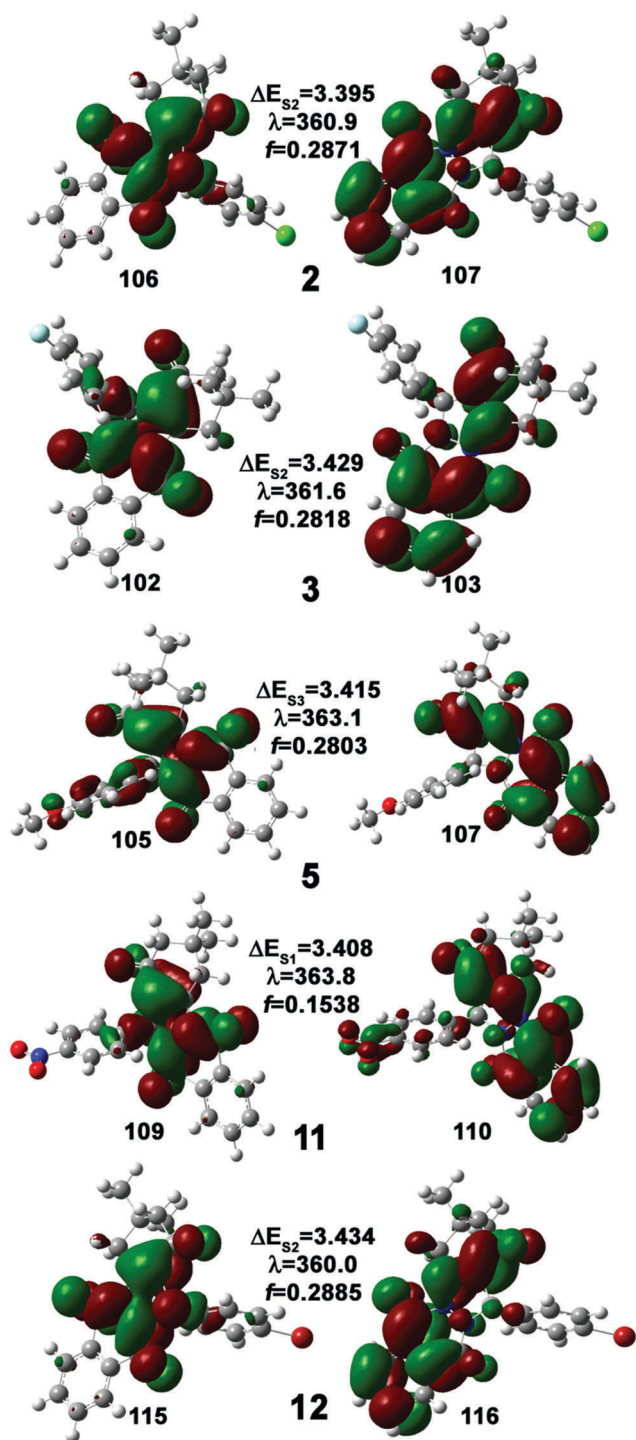


Fig. 9 Molecular orbitals involved in the time-dependent DFT calculated [B3LYP/6-31G(d,p)] transition with the largest oscillator strength (f) for phthalazine-triones whose crystal structures were determined here (2, 5 and 11) and those previously elucidated (3 and 12).^{5,19} The highest occupied molecular orbital (HOMO) [or HOMO-1 in 5] and the lowest unoccupied molecular orbital (LUMO) are on the left and right columns and mean the ground and excited states, respectively. The transition energy and wavelength are in eV and nm, respectively.

Even though PL seems to be mainly related to the presence of an intramolecular core conserved in our compounds, the control of light emission features by crystalline materials has been obtained with an adequate choice of intermolecular interactions. This has been commonly employed in single-component crystal forms, including polymorphs and multi-component crystal forms.²³ Crystal engineers use several types of intermolecular interactions to tune emission wavelength, lifetime and efficiency. A few of those intermolecular interactions include halogen...hydrogen and lone pair...halogen bonds,²⁴ classical hydrogen bonds,²⁵ π - π interactions and stacking fashions.^{25,26} Even the enhancement of excited state intramolecular proton transfer (ESIPT), a photochemical process much invoked to improve light-emitting properties, can be demonstrated through non-classical hydrogen bonds and π - π interactions in the solid state.²⁷

The observation that PL arose from the phthalazine-trione moiety was supported by our TD-DFT calculations for all phthalazine-triones whose crystal geometries were available. After their full geometric optimization, the electronic transitions with the largest oscillator strengths were found near 360 nm, in excellent agreement with the excitation energy. In all compounds, the FMOs involved in these excitations were distributed over the phthalazine-trione moiety and were not localized on the C15 substituent (Fig. 9). Therefore, we demonstrate that the phthalazine-trione moiety is a promising fluorophore in the blue-green spectral regions. At last, compound 11 was not photoluminescent, which is due to the strong self-absorption from the NO₂ group in the visible emission region.²⁸

The transmission spectra of ten compounds in a formaldehyde solution (0.1 mmol L⁻¹) are shown in Fig. 10. All compounds presented similar absorption bands in the range from 240 to 440 nm, having two main absorptions at ~250 nm and ~370 nm (with some lateral absorption). A strong and broad absorption band around 370 nm was in good agreement with the calculations shown in Fig. 9, which illustrated the largest oscillator strengths near 360 nm due to the HOMO-LUMO transition placed over the phthalazine-trione moiety.

We present in Fig. 11(a) the PL emission spectra for samples 1 to 10 in formaldehyde solution (0.1 mmol L⁻¹), under

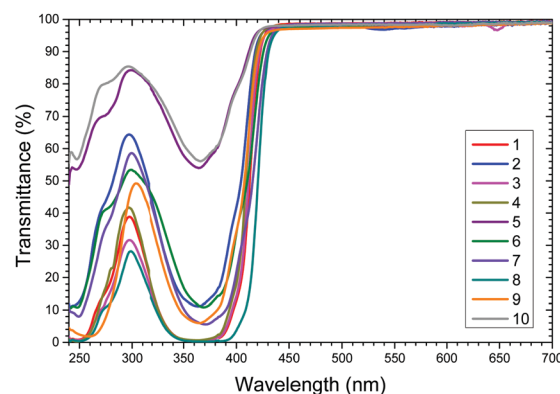
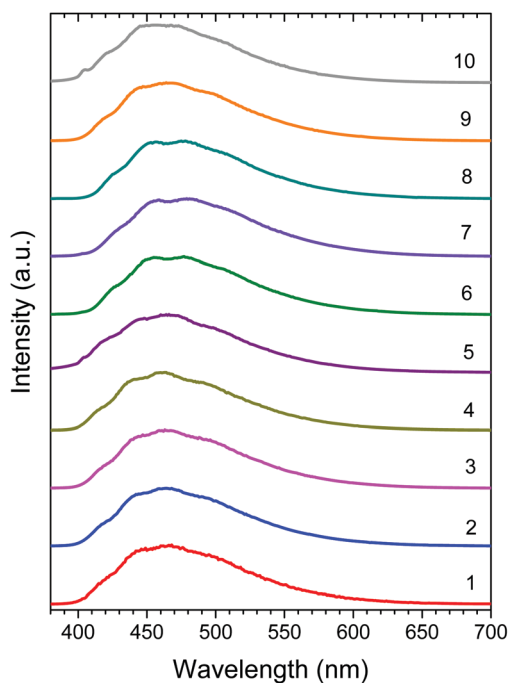
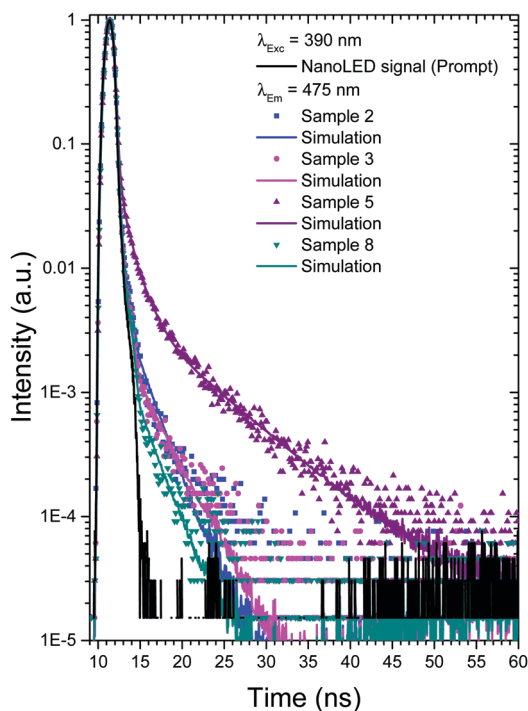


Fig. 10 Transmittance spectra of the ten phthalazine-triones studied here in a formaldehyde solution (0.1 mmol L⁻¹).

excitation at 360 nm using a continuous Xe arc lamp. Broad band emissions were observed from 400 to 600 nm with the



(a)



(b)

Fig. 11 (a) PL emission spectra of **1** to **10** in a formaldehyde solution (0.1 mmol L^{-1}), under excitation at 360 nm using a continuous Xe arc lamp. (b) PL decay curves of **2**, **3**, **5** and **8** under excitation at 390 nm using a NanoLED source (1 MHz and peak pulse of 1.2 ns) and monitoring emission at 475 nm with a bandpass of 6 nm.

Table 4 Lifetime values of **2**, **3**, **5** and **8** under excitation at 390 nm using a NanoLED source (1 MHz and peak pulse of 1.2 ns) and monitoring emission at 475 nm with a bandpass of 6 nm

Sample	τ_1 (ns)	τ_2 (ns)	A_1	A_2	χ^2
2	2.33 ± 0.04	—	1.00	0	1.81
3	3.21 ± 0.06	—	1.00	0	1.53
5	1.59 ± 0.02	7.87 ± 0.06	0.68	0.32	1.64
8	2.46 ± 0.06	—	1.00	0	1.39

maximum around 475 nm, and all samples have a similar spectral shape. Some samples presented a PL emission spectrum shifted slightly to the red region (**6**, **7** and **8**), which can be related to the substituent at C15 (*n*-propyl in **6**, cyclohexyl in **7**, and *n*-butyl in **8**). All PL emission spectra for compounds dissolved in formaldehyde were similar to those in the solid state. However, the PL emission spectra were broader, as expected, due to interactions with solvent molecules.

PL emission decay curves for four selected samples (**2**, **3**, **5** and **8**) are illustrated in Fig. 11(b). These curves could be well-fitted with exponential functions:

$$I(t) = A_1 e^{-t/\tau_1} + A_2 e^{-t/\tau_2} \quad (1)$$

All fittings are illustrated in Fig. 11(b) and the parameters are listed in the Table 4. The quality of the fittings was measured by χ^2 , and all values were between 1.39 and 1.81, close to unity. Samples **2**, **3** and **8** possessed only one component, with a lifetime between 2.33 and 3.21 ns. However, sample **5** possessed two components, one at 1.59 ns and another at 7.87 ns. All these results corroborate that the main emissions are due to HOMO–LUMO transitions distributed over the phthalazine-trione rings. The second component of **5** may be attributed to the 3-methoxyphenyl substituent. Indeed, HOMO–1 was also slightly distributed over this substituent in **5** (Fig. 9), which therefore contributed to the main transition calculated by TD-DFT.

Conclusions

In this study, we determined the crystal structures of three phthalazine-triones discovering interesting relationships between the conformation of their rings and between these conformations and the intermolecular interaction patterns. Furthermore, these interplays could be better understood by comparing crystal geometries to theoretical geometries calculated in the gas phase. However, the main contribution of this study is the discovery of a new class of blue and green light emitting compounds. These compounds have conserved the luminescence profile since this optical property came from their common phthalazine-trione moiety. Our theoretical approaches using time-dependent DFT allowed us to conclude that the main transition responsible for the observed emissions involves FMOs distributed over this common moiety although they are not localized on the changeable substituent. The absorption bands, PL emission and lifetime of compounds were evaluated, the results of which correlated well with the TD-DFT results. Similar PL emission spectra were

observed in solution and solid-state phases. The main lifetime of emissions at 475 nm were between 1.59 ns and 3.21 ns due to HOMO–LUMO transitions. Therefore, this study contributes significantly to the material chemistry field by sourcing a new robust fluorophore that can be further explored to conceive blue-green light-emitting devices.

Conflicts of interest

There are no conflicts to declare.

Acknowledgements

The authors acknowledge CNPq, CAPES, FAPEMIG and FAPEG for financial support and research fellowships. This study was financed in part by the Coordenação de Aperfeiçoamento de Pessoal de Nível Superior – Brasil (CAPES) – Finance Code 001.

Notes and references

- 1 C. K. Ryu, R. E. Park, M. Y. Ma and J. H. Nho, *Bioorg. Med. Chem. Lett.*, 2007, **17**, 2577–2580.
- 2 M. A. J. Duncton, E. L. PiatnitskiChekler, R. Katoch-Rouse, D. Sherman, W. C. Wong, L. M. Smith, J. K. Kawakami, A. S. Kiselyov, D. L. Milligan, C. Balagtas, Y. R. Hadari, Y. Wang, S. N. Patel, R. L. Rolster, J. R. Tonra, D. Surguladze, S. Mitelman, P. Kussie, P. Bohlen and J. F. Doody, *Bioorg. Med. Chem.*, 2009, **17**, 731–740.
- 3 F. M. Awadallah, W. I. El-Eraky and D. O. Saleh, *Eur. J. Med. Chem.*, 2012, **52**, 14–21.
- 4 N. Watanabe, Y. Kabasawa, Y. Takase, M. Matsukura, K. Miyazaki, H. Ishihara, K. Kodama and H. Adachi, *J. Med. Chem.*, 1998, **41**, 3367–3372.
- 5 Y. F. Rego, C. M. da Silva, D. L. da Silva, J. G. da Silva, A. L. T. G. Ruiz, J. E. de Carvalho, S. A. Fernandes and Â. de Fátima, *Arabian J. Chem.*, DOI: 10.1016/j.arabjc.2016.04.007.
- 6 E. C. Lim and J. Stanislaus, *J. Chem. Phys.*, 1970, **53**, 2096–2100.
- 7 T. M. H. Vuong, J. Weimmerskirch-Aubatin, J.-F. Lohier, N. Bar, S. Boudin, C. Labbé, F. Gourbilleau, H. Nguyen, T. T. Dang and D. Villemin, *New J. Chem.*, 2016, **40**, 6070–6076.
- 8 L. Xin, J. Xue, G. Lei and J. Qiao, *RSC Adv.*, 2015, **5**, 42354–42361.
- 9 B. Liu, M. Xu, H. Tao, L. Ying, J. Zou, H. Wu and J. Peng, *J. Lumin.*, 2013, **142**, 35–39.
- 10 X. Shi, M. Ding, C. Li, W. Wang and H. Guo, *J. Heterocycl. Chem.*, 2018, **55**, 440–446.
- 11 SADABS, APEX2 and SAINT, Bruker AXS Inc., Madison, Wisconsin, USA, 2009.
- 12 L. Krause, R. Herbst-Irmer, G. M. Sheldrick and D. Stalke, *J. Appl. Crystallogr.*, 2015, **48**, 3–10.
- 13 G. M. Sheldrick, *Acta Crystallogr., Sect. C: Struct. Chem.*, 2015, **71**, 3–8.
- 14 L. J. Farrugia, *J. Appl. Crystallogr.*, 1999, **32**, 837.
- 15 C. F. Macrae, I. J. Bruno, J. A. Chisholm, P. R. Edgington, P. McCabe, E. Pidcock, L. Rodriguez-Monge, R. Taylor, J. Van De Streek and P. A. Wood, *J. Appl. Crystallogr.*, 2008, **41**, 466–470.
- 16 L. J. Farrugia, *J. Appl. Crystallogr.*, 1997, **30**, 565.
- 17 P. Hohenberg and W. Kohn, *Phys. Rev.*, 1964, **136**, B864–B871.
- 18 W. Kohn and L. J. Sham, *Phys. Rev.*, 1965, **140**, A1133–A1138.
- 19 M. Sayyafi, M. Seyyedhamzeh, H. R. Khavasi and A. Bazgir, *Tetrahedron*, 2008, **64**, 2375–2378.
- 20 A. D. Becke, *J. Chem. Phys.*, 1993, **98**, 5648–5652.
- 21 C. Lee, W. Yang and R. G. Parr, *Phys. Rev. B: Condens. Matter Phys.*, 1988, **37**, 785–789.
- 22 M. J. Frisch, G. W. Trucks, H. B. Schlegel, G. E. Scuseria, M. A. Robb, J. R. Cheeseman, G. Scalmani, V. Barone, B. Mennucci, G. A. Petersson, H. Nakatsuji, M. Caricato, X. Li, H. P. Hratchian, A. F. Izmaylov, J. Bloino, G. Zheng, J. L. Sonnenberg, M. Hada, M. Ehara, K. Toyota, R. Fukuda, J. Hasegawa, M. Ishida, T. Nakajima, Y. Honda, O. Kitao, H. Nakai, T. Vreven, J. A. Montgomery Jr., J. E. Peralta, F. Ogliaro, M. Bearpark, J. J. Heyd, E. Brothers, K. N. Kudin, V. N. Staroverov, R. Kobayashi, J. Normand, K. Raghavachari, A. Rendell, J. C. Burant, S. S. Iyengar, J. Tomasi, M. Cossi, N. Rega, J. M. Millam, M. Klene, J. E. Knox, J. B. Cross, V. Bakken, C. Adamo, J. Jaramillo, R. Gomperts, R. E. Stratmann, O. Yazyev, A. J. Austin, R. Cammi, C. Pomelli, J. W. Ochterski, R. L. Martin, K. Morokuma, V. G. Zakrzewski, G. A. Voth, P. Salvador, J. J. Dannenberg, S. Dapprich, A. D. Daniels, O. Farkas, J. B. Foresman, J. V. Ortiz, J. Cioslowski and D. J. Fox, *Gaussian 09*, Gaussian Inc., Wallingford, CT, 2009.
- 23 D. Yan and D. G. Evans, *Mater. Horiz.*, 2014, **1**, 46–57.
- 24 D. Yan, H. Yang, Q. Meng, H. Lin and M. Wei, *Adv. Funct. Mater.*, 2014, **24**, 587–594.
- 25 G. Fan and D. Yan, *Sci. Rep.*, 2014, **4**, 4933.
- 26 D. Yan, B. Patel, A. Delori, W. Jones and X. Duan, *Cryst. Growth Des.*, 2013, **13**, 333–340.
- 27 H. Lin, X. Chang, D. Yan, W.-H. Fang and G. Cui, *Chem. Sci.*, 2017, **8**, 2086–2090.
- 28 T. E. Souza, I. M. L. Rosa, A. O. Legendre, D. Paschoal, L. J. Q. Maia, H. F. dos Santos, F. T. Matins and A. C. Doriguetto, *Acta Crystallogr., Sect. B: Struct. Sci., Cryst. Eng. Mater.*, 2015, **71**, 416–426.